

THE DENSITY VARIANCE–MACH NUMBER RELATION IN SUPERSONIC, ISOTHERMAL TURBULENCE

DANIEL J. PRICE¹, CHRISTOPH FEDERRATH^{2,4}, AND CHRISTOPHER M. BRUNT³

¹ Centre for Stellar and Planetary Astrophysics, School of Mathematical Sciences, Monash University, Clayton, Vic 3168, Australia; daniel.price@monash.edu

² Zentrum für Astronomie der Universität Heidelberg, Institut für Theoretische Astrophysik, Albert-Ueberle-Str. 2, D-69120 Heidelberg, Germany

³ School of Physics, University of Exeter, Stocker Rd, Exeter EX4 4QL, UK

Received 2010 September 10; accepted 2010 December 13; published 2010 December 29

ABSTRACT

We examine the relation between the density variance and the mean-square Mach number in supersonic, isothermal turbulence, assumed in several recent analytic models of the star formation process. From a series of calculations of supersonic, hydrodynamic turbulence driven using purely solenoidal Fourier modes, we find that the “standard” relationship between the variance in the log of density and the Mach number squared, i.e., $\sigma_{\ln \rho/\bar{\rho}}^2 = \ln(1 + b^2 \mathcal{M}^2)$, with $b = 1/3$, is a good fit to the numerical results in the supersonic regime up to at least Mach 20, similar to previous determinations at lower Mach numbers. While direct measurements of the variance in linear density are found to be severely underestimated by finite resolution effects, it is possible to infer the linear density variance via the assumption of log-normality in the probability distribution function. The inferred relationship with Mach number, consistent with $\sigma_{\rho/\bar{\rho}} \approx b\mathcal{M}$ with $b = 1/3$, is, however, significantly shallower than observational determinations of the relationship in the Taurus Molecular Cloud and IC5146 (both consistent with $b \approx 0.5$), implying that additional physics such as gravity is important in these clouds and/or that turbulent driving in the interstellar medium contains a significant compressive component. Magnetic fields are not found to change this picture significantly, in general reducing the measured variances and thus worsening the discrepancy with observations.

Key words: hydrodynamics – ISM: structure – magnetohydrodynamics (MHD) – shock waves – stars: formation – turbulence

Online-only material: color figures

1. INTRODUCTION

The last few years have seen an increasing number of analytic models of the star formation process that use the log-normal density probability distribution function (PDF) produced by supersonic turbulent flows to predict statistical quantities such as the initial and/or core mass function (e.g., Padoan & Nordlund 2002; Hennebelle & Chabrier 2008, 2009) and the star formation rate (Krumholz & McKee 2005; Padoan & Nordlund 2009). A key assumption in these models is a relationship identified in early numerical studies between the PDF width—the density variance or standard deviation—and the root-mean-square (rms) Mach number \mathcal{M} in supersonic, isothermal turbulence. The relationship is generally assumed to be linear in the standard deviation of linear density, i.e.,

$$\sigma_{\rho/\bar{\rho}} = b\mathcal{M}, \quad (1)$$

where b is a constant of order unity and density is scaled in terms of the mean, $\bar{\rho}$. For a log-normal distribution, this is equivalent to

$$\sigma_s^2 = \ln(1 + b^2 \mathcal{M}^2), \quad (2)$$

where $s \equiv \ln(\rho/\bar{\rho})$, such that σ_s is the standard deviation in the logarithm of density.

Apart from the early empirical findings of Vázquez-Semadeni (1994), Padoan et al. (1997b), and Passot & Vázquez-Semadeni (1998), there is no clear reason why the relationship should be of this form. Mathematically, the appearance of a log-normal distribution can be understood as a consequence of the multiplicative central limit theorem assuming that individual

density perturbations are independent and random (Vázquez-Semadeni 1994; Passot & Vázquez-Semadeni 1998; Nordlund & Padoan 1999). In physical terms this has been interpreted as meaning that density fluctuations at a given location are constructed by successive passages of shocks with a jump amplitude independent of the local density (e.g., Ballesteros-Paredes et al. 2007; Kritsuk et al. 2007; Federrath et al. 2010). However, it has not so far proved possible to analytically predict the relationship based on these ideas (though see Padoan & Nordlund 2009). Thus, a common approach in numerical studies of turbulence—usually at a fixed Mach number—has been to measure the parameter b , assuming Equation (2), that gives best-fitting log-normal to the time-averaged PDF. However, reported estimates for b are widely discrepant. For example, Padoan et al. (1997b) found $b \approx 0.5$ while more recently Kritsuk et al. (2007) (at Mach 6) find a much lower value of $b \approx 0.26$ and Beetz et al. (2008) find $b \approx 0.37$, while Passot & Vázquez-Semadeni (1998) found $b \approx 1$ (though with some confusion over σ_s versus $\sigma_{\rho/\bar{\rho}}$).

Federrath et al. (2008) and Federrath et al. (2010) reconcile these results in part by the finding that the width of the PDF depends not only on the rms Mach number but also on the relative degree of compressible and solenoidal modes in the turbulence forcing, with $b = 1/3$ appropriate for purely solenoidal and $b = 1$ for purely compressive forcing. This is in keeping with earlier discussions by Passot & Vázquez-Semadeni (1998) and Nordlund & Padoan (1999, p. 222), the latter authors noting that “for compressional forcing at low Mach numbers (leading to an ensemble of sound waves), the standard deviation is expected to be equal to the rms Mach number itself.”

Observationally, the log-normality of the three-dimensional (3D) PDF is reflected in the two-dimensional (2D) column density PDF, for example, as measured from dust extinction maps (e.g., Lombardi et al. 2006, 2008, 2010; Kainulainen

⁴ Current address: Ecole Normale Supérieure de Lyon, CRAL, 69364 Lyon Cedex 07, France.

et al. 2009)—at least in earlier stages of molecular cloud evolution, suggesting that this phase could be dominated by roughly isothermal turbulence in which self-gravity is relatively unimportant. Only for seemingly more evolved clouds (including Taurus) do Kainulainen et al. (2009) see significant tails at higher (column) densities (similarly found by Lombardi et al. 2010). However, measurements of the projected 2D variance (or PDF) cannot be directly used to constrain the relationship with Mach number. Recently, Brunt et al. (2010a, hereafter BFP) have shown how projection effects can be overcome to infer the 3D density variance from column density observations, in turn leading to a method for extracting the unprojected (3D) density PDF from the observational data (Brunt et al. 2010b). This enables the relationship between the standard deviation in linear density and Mach number to be tested observationally, with initial application to Taurus finding $b = 0.48^{+0.15}_{-0.11}$ (Brunt 2010). A similar method was employed by Padoan et al. (1997a) to infer the 3D density variance from extinction measurements in IC5146, similarly finding $b \approx 0.5$.

The problem with all of the above is that calculations—or observations—performed at a single (rms) Mach number can only ever assume the relationship given by Equation (2) or Equation (1) and cannot be used to constrain it unless a range of Mach numbers are studied. Indeed, Lemaster & Stone (2008, hereafter LS08)—performing a series of calculations with Mach numbers in the range $1.2 \leq \mathcal{M} \leq 6.8$ —find a relationship

$$\sigma_s^2 = 0.72 \ln(1 + 0.5\mathcal{M}^2) - 0.20, \quad (3)$$

based on a fit to measurements of the mean in the logarithm of density, \bar{s} , as a function of \mathcal{M} , which we have here converted to a σ_s - \mathcal{M} relation using $\bar{s} = -\sigma_s^2/2$. However, this three-parameter fit is clearly not unique, and it remains to be determined whether this or a similar relationship continues to hold at higher Mach numbers.

The present study is motivated by a need to compare the theoretical predictions with the observational constraints. In particular, LS08 only perform calculations up to $\mathcal{M} \approx 6.8$ —corresponding to one-dimensional (1D) line full width at half-maximum of $\sim 1.6 \text{ km s}^{-1}$ (at 10 K), which is rather low in terms of what is found in the real interstellar medium (ISM). In particular, Taurus has $\mathcal{M} \sim 17$, so a study going up to (at least) Mach 20 or so is needed. Our aim in this Letter is precisely this: to pin down the theoretical relationship—with as few assumptions as possible—up to sufficiently high Mach numbers that a meaningful comparison can be made with observed molecular clouds. While additional physics such as non-isothermality (e.g., Scalo et al. 1998), the multiphase nature of the ISM, and self-gravity (e.g., Klessen 2000; Kritsuk et al. 2010) are all expected to change the theoretical predictions at some level, the isothermal, non-self-gravitating case is an important reference point that remains theoretically uncertain. Furthermore, a clear prediction for this simple case can be used to gauge the relative importance of such additional physics in observed clouds.

2. METHODS

2.1. Log-normal Distributions

The log-normal distribution is given by

$$p(s)ds = \frac{1}{\sqrt{2\pi}\sigma_s} \exp\left[-\frac{1}{2}\left(\frac{s-\bar{s}}{\sigma_s}\right)^2\right] ds, \quad (4)$$

where $s \equiv \ln(\rho/\bar{\rho})$ such that \bar{s} and σ_s denote the mean and standard deviation in the logarithm of (scaled) density, respectively, and $\bar{\rho}$ is the mean in the linear density. The mean and variances in a log-normal distribution are related by

$$\bar{s} = -\frac{1}{2}\sigma_s^2, \quad (5)$$

and

$$\sigma_{\rho/\bar{\rho}}^2 = \exp(\sigma_s^2) - 1. \quad (6)$$

2.2. Numerical Simulations

We have performed a series of calculations of supersonic turbulence, solving the equations of compressible hydrodynamics using an isothermal equation of state (with sound speed $c_s = 1$) and periodic boundary conditions in the 3D domain $x, y, z \in [0, 1]$. Initial conditions were a uniform density medium $\rho = \bar{\rho} = 1$ with zero initial velocities. Turbulence was produced by adding a random, correlated stirring force, driving the few largest Fourier modes $1 < k < 3$ with a random forcing pattern, slowly changed according to an Ornstein–Uhlenbeck (OU) process, such that the pattern evolves smoothly in space and time (Schmidt et al. 2009; Federrath et al. 2010). The driving, and the PHANTOM smoothed particle hydrodynamics (SPH) code employed, is described in detail in Price & Federrath (2010, hereafter PF10; see also Federrath et al. 2010). Calculations were evolved for 10 dynamical times (defined as $t_d \equiv L/(2\mathcal{M}c_s)$), using only results after $2t_d$ such that turbulence is fully established (e.g., Federrath et al. 2009). The amplitude of the driving force was adjusted to give rms Mach numbers in the range $1 \leq \mathcal{M} \leq 20$ by varying the energy input per Fourier mode proportional to the Mach number squared, i.e., $E_{\text{stir}} \propto \mathcal{M}^2$ while the correlation time for the OU process was set to t_d (for the nominally input \mathcal{M}).

Most importantly, unless otherwise specified we have driven the turbulence using purely solenoidal Fourier modes. Thus, according to the heuristic theory of Federrath et al. (2010) we should expect a relationship of the standard form (2) with $b \approx 1/3$.

2.3. Measuring the Density Variance

We consider a range of methods for measuring the density variance from the simulations.

1. Measure the linear variance, $\sigma_{\rho/\bar{\rho}}^2$, directly—with no assumptions about log-normality or otherwise—and fit the measured relation as a function of \mathcal{M} .
2. Measure the logarithmic variance σ_s^2 directly and fit the measured relation. Infer $\sigma_{\rho/\bar{\rho}}$ assuming a log-normal PDF via Equation (6).
3. Measure \bar{s} and fit the measured relation. Infer σ_s using Equation (5) and in turn $\sigma_{\rho/\bar{\rho}}$ using Equation (6).
4. Determine the value of σ_s that gives the best-fitting PDF in a restricted range around the mean. Infer $\sigma_{\rho/\bar{\rho}}$ using Equation (6).

The objection to method 1 is that it is sensitive to the tails of the density distribution, where time-dependent fluctuations and intermittency effects can cause deviations from log-normality (Kritsuk et al. 2007; Federrath et al. 2010; PF10). On the other hand, no assumptions are made regarding the PDF, while methods 2–4 assume a priori that the PDF is log-normal, though for methods 2 and 3 only for obtaining the linear variance. Method 4 is the usual approach used to fit b for a given Mach

number, if one additionally assumes the relationship given by Equation (2)—an assumption we do not need to make here since a range of Mach numbers are examined.

While the results are discussed in more detail below, essentially we find that methods 1–4 all give similar results for σ_s , independent of numerical resolution, but that direct measurements of $\sigma_{\rho/\bar{\rho}}$ (method (1)) are highly resolution dependent.

Volume-weighted variances were computed from the (mass-weighted) SPH data by interpolating the density field to a grid. We found that this procedure gave better results than the direct calculation from the particles we have previously advocated (PF10), particularly at high Mach numbers ($\mathcal{M} \gtrsim 10$) where assuming that the volume element m/ρ is constant over the smoothing radius is an increasingly poor approximation. However, capturing the full resolution in the density field was found to require an adaptive rather than fixed mesh.

All plots show volume-weighted quantities, time-averaged over 81 snapshots evenly spaced between $t/t_d = 2$ and $t/t_d = 10$, with error bars showing the (temporal) 1σ deviations from these values.

3. DENSITY VARIANCE–MACH NUMBER RELATION IN SUPERSONIC, ISOTHERMAL TURBULENCE

3.1. σ_s as a Function of \mathcal{M}

The direct measurements of the standard deviation in the log density, σ_s , are shown in Figure 1 from the results of calculations performed using 128^3 , 256^3 , and 512^3 SPH particles, using methods (2) and (4) (see the legend). Dashed lines show the standard relation (Equation (2)) with $b = 1/3$ and $b = 1/2$, while the dotted line shows the best-fitting relationship found by LS08 (Equation (3)). Both the $b = 1/3$ curve, expected for solenoidally driven turbulence (Federrath et al. 2008, 2010) and the LS08 fit show reasonable fits to the data, and indeed cannot be distinguished given the time variability present in the calculations. However, adopting $b = 0.5$ is clearly not consistent with our solenoidally driven results. The results are also consistent with our earlier findings (PF10), that showed a convergence in both grid and SPH methods toward $b \approx 0.35$ – 0.4 at Mach 10.

The measured value of σ_s cannot be compared to observations, since only the 3D variance in the linear density can be observationally inferred (e.g., using the BFP method). Thus, it is necessary to either measure or infer the linear variance from simulations to make this comparison.

3.2. Direct Measurement of $\sigma_{\rho/\bar{\rho}}$

A direct measurement of the linear density variance is difficult even with high-resolution simulations, demonstrated in Figure 2, that shows the directly measured $\sigma_{\rho/\bar{\rho}}^2$ as a function of σ_s^2 . The dashed line shows the expected relationship for a log-normal distribution (Equation (6)). The exponential relationship is resolved only at the lowest Mach numbers, $\mathcal{M} \lesssim 5$, corresponding to $\sigma_s^2 \lesssim 1.4$, while at higher Mach numbers $\sigma_{\rho/\bar{\rho}}$ is a strong function of resolution, most easily demonstrated by interpolating the highest resolution SPH calculations (512^3 particles) to fixed grids of decreasing resolution (see the legend). This dependence is the reason why we eventually interpolated the SPH data onto an adaptive mesh, refined such that $\Delta x < h$ for all cells within the smoothing radius $2h$ of any given particle, in order to obtain a result for $\sigma_{\rho/\bar{\rho}}$ that captures the maximum resolution available in the SPH simulations, though we remain limited by the intrinsic resolution of the simulations. PF10

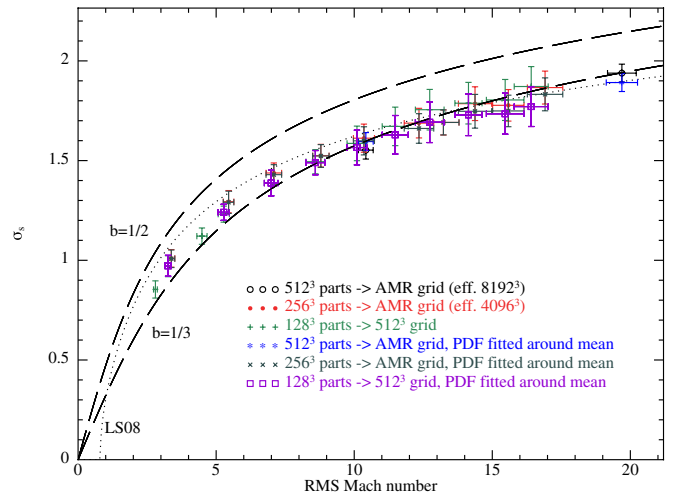


Figure 1. Measured relationship between the (volume-weighted) standard deviation of the logarithm of density σ_s as a function of rms Mach number from a series of solenoidally driven supersonic turbulence calculations. The points show time averages, with error bars showing the (temporal) 1σ deviations. The dashed lines show the standard relation (Equation (2)) with $b = 1/3$ and $b = 1/2$, while the dotted line shows the best-fitting relationship found by Lemaster & Stone (2008; Equation (3)). Differences between directly measuring σ_s (open circles, filled circles, and plus signs) compared to fitting the PDF around the mean (*, ×, and squares) are not significant (i.e., smaller than the time-dependent fluctuations). Overall, the results are consistent with $b = 1/3$, as expected for solenoidally driven turbulence from Federrath et al. (2008, 2010), and indistinguishable from the LS08 best fit.

(A color version of this figure is available in the online journal.)

found that SPH simulations at Mach 10 resolved a maximum density at 128^3 particles similar to that captured on a fixed grid at 512^3 grid cells. This is consistent with the results here, where it is necessary to refine the grid to an effective 8192^3 for the Mach 20 calculations employing 512^3 SPH particles. It is also evident that fully resolving the strong fluctuations in the linear density at high Mach number is intractable with current computational resources. Our findings also suggest that the linear density variance is likely to be severely underestimated by limited observational resolution, so the results in Taurus and IC5146 are almost certainly lower limits (see also Brunt 2010).

3.3. $\sigma_{\rho/\bar{\rho}}$ as a Function of \mathcal{M} : Comparison to Observations

The direct—but resolution limited—measurements for $\sigma_{\rho/\bar{\rho}}$, computed without assumptions from the adaptive mesh refinement (AMR) grid, are shown in Figure 3 (see the legend, i.e., method (1) above). A better approach is to use the fact that the measurements for σ_s are resolution independent (Figure 1), meaning that we can use the assumption of log-normality to infer the fully resolved value for $\sigma_{\rho/\bar{\rho}}$, i.e., using Equation (6) (method 2). The standard deviations computed in this way are also shown and as expected are consistent with a linear $\sigma_{\rho/\bar{\rho}}-\mathcal{M}$ relation with $b = 1/3$ for solenoidal forcing (Federrath et al. 2008, 2010), and also with the LS08 best fit, the latter translated in terms of $\sigma_{\rho/\bar{\rho}}$ using Equation (6).

We are now in a position to compare with the observational results. It should first be noted that the assumption of the $\sigma_s-\sigma_{\rho/\bar{\rho}}$ relation for the simulations essentially gives us an upper limit on $\sigma_{\rho/\bar{\rho}}$, whereas (see above) the finite resolution of the observations almost certainly gives a lower limit on the variance. The results from Padoan et al. (1997a; in IC5146: $b = 0.5 \pm 0.05$ at Mach 10) and Brunt (2010; in Taurus, $\mathcal{M}_{\text{rms}} = 17.6 \pm 1.8$ and $\sigma_{\rho/\bar{\rho}} = 8.49_{-1.71}^{+1.85}$) are also plotted, both of which are consistent

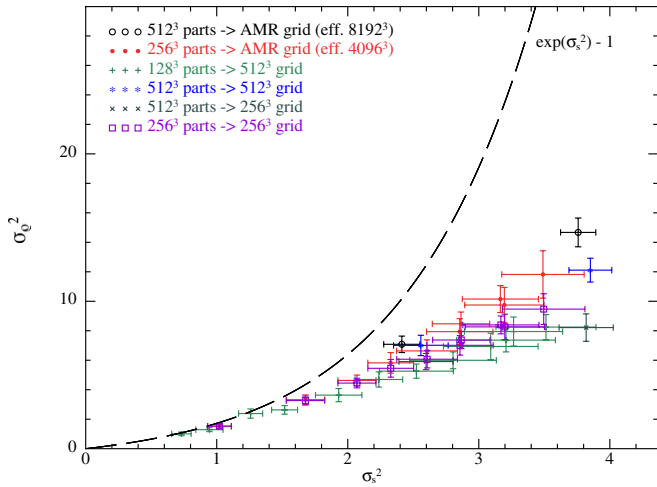


Figure 2. Relationship between the linear and logarithmic density variance as a function of both intrinsic SPH resolution (number of particles) and the grid size used to compute the variances (see the legend). While the measurements of σ_s^2 are resolution independent, there is a strong dependence on both the SPH and grid resolution in the directly measured linear variance, $\sigma_{\rho/\bar{\rho}}^2$. Using an AMR grid to compute volume-weighted variances captures the full density field resolution in the SPH simulations, but even in the highest resolution calculations (512³ particles), $\sigma_{\rho/\bar{\rho}}^2$ is severely underestimated compared to the expected exponential relationship (Equation (6), dashed line) for $\mathcal{M} \gtrsim 5$.

(A color version of this figure is available in the online journal.)

with $b = 0.5$ but clearly inconsistent with the calculations of purely solenoidally driven turbulence.

The other extreme is given by the $b = 1$ line in Figure 3, corresponding to purely compressive forcing (Federrath et al. 2008, 2010). Data points from two 1024³ grid simulations of purely solenoidal and purely compressive forcing by Federrath et al. (2008, 2010) are also shown (cyan triangles). Clearly, purely solenoidal and purely compressive forcing seem inconsistent with the observations, while a mixture and/or the addition of gravity can fit the observations, best fit by a linear relation with $b \approx 0.5$. The σ_ρ - \mathcal{M} plane, however, needs to be populated with many more observational measures to draw more definite conclusions about, e.g., regional and evolutionary variations.

4. DENSITY VARIANCE-MACH NUMBER RELATION IN MHD TURBULENCE

Since molecular clouds are observed to be magnetized, we have additionally computed a series of magnetohydrodynamics (MHD) calculations, driven identically to their hydrodynamic counterparts but with an initially uniform magnetic field threading the box. These have been computed on a fixed grid using the FLASH code, as described in Federrath et al. (2010), PF10, and Brunt et al. (2010a, 2010b); note that the driving routines are implemented identically in both the SPH and grid code). The magnetic field strength in the MHD calculations is characterized by the ratio of gas-to-magnetic pressure $\beta = P/P_{\text{mag}}$ in the initial conditions, where $P_{\text{mag}} = \frac{1}{2}B^2/\mu_0$. As done previously, we have also examined the effect of resolution, with a finding similar to the hydrodynamic case, namely, that direct measurements of $\sigma_{\rho/\bar{\rho}}$ are strongly resolution affected (underestimated)—even at modest Mach numbers, similar to the results shown in Figure 2, but that measurements of σ_s are resolution independent (at $\gtrsim 256^3$ grid cells).

Figure 4 shows the results, similar to Figure 1 for the hydrodynamic case and overplotted with the hydrodynamic

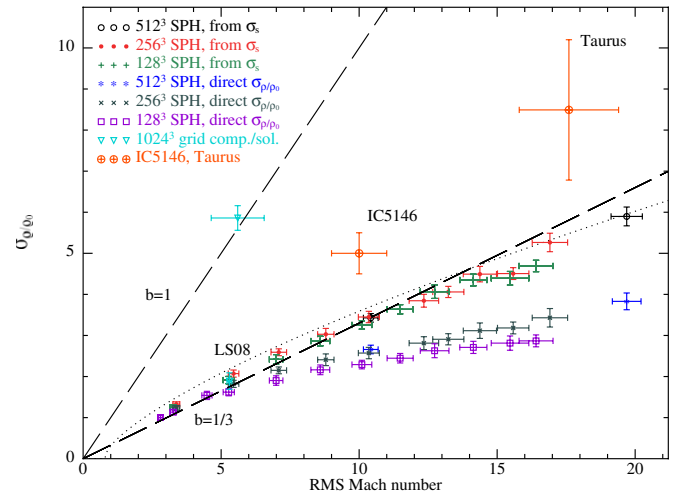


Figure 3. Directly measured or inferred (see the legend) standard deviation of the linear density $\sigma_{\rho/\bar{\rho}}$ as a function of rms Mach number from the solenoidally driven supersonic turbulence calculations. For comparison, observational determinations by Padoan et al. (1997a) and Brunt (2010) in IC5146 and Taurus (respectively) are shown, together with the expected $b = 1/3$ and $b = 1$ linear relationships for solenoidal and compressive forcing (respectively; Federrath et al. 2008, 2010), including the corresponding data points from Federrath et al. (2010; 1024³ grid; cyan triangles). Direct measurements of $\sigma_{\rho/\bar{\rho}}$ are resolution limited (see Figure 2), although the values inferred by assuming Equation (6) are upper limits, whereas the observations are likely to be lower limits. The discrepancy between solenoidally driven simulations and observations indicates that some amount of gravity and/or compressive driving is necessary to explain the observational results.

(A color version of this figure is available in the online journal.)

$b = 1/3$ and $b = 1/2$ relationships (dashed lines) as well as the best-fitting MHD relationship found by LS08. The most obvious difference with MHD is that the density variances are significantly lower than their hydrodynamic counterparts at high (sonic) Mach number $\mathcal{M} \gtrsim 10$ —though conversely marginally higher at lower Mach numbers. On the whole increasing the field strength seems to decrease the mean σ_s slightly. While a complete MHD study is beyond the scope of this Letter, the results clearly illustrate a shallower relationship than the hydrodynamic $b = 1/3$ curve at high Mach number, with σ_s only weakly dependent on \mathcal{M} in this regime (for $\beta \lesssim 1$). Thus, if anything, adding magnetic fields decreases the variance in the density field, worsening the discrepancy with observations.

5. CONCLUSIONS

We have measured the relationship between the density variance and the mean-square Mach number from a series of simulations of supersonic, isothermal, solenoidally driven turbulence over a wide range of Mach numbers ($1 \lesssim \mathcal{M} \lesssim 20$). We find that the standard relationship given by Equation (2) with $b = 1/3$ provides a good fit to the data over this range, consistent with the heuristic theory of Federrath et al. (2010) for solenoidal driving and with similar measurements by Lemaster & Stone (2008) at lower Mach numbers. While it is difficult to measure the variance in linear density directly from simulations with finite resolution, the inferred relationship (Equation (1), with $b = 1/3$) appears inconsistent with observational determinations ($b \approx 0.5$) in Taurus and IC5146, suggesting that additional physics such as gravity is important in these clouds and/or that some form of compressive driving is relevant. This is consistent with the findings of Kainulainen et al. (2009) and Lombardi et al. (2010) for Taurus, where self-gravity is invoked

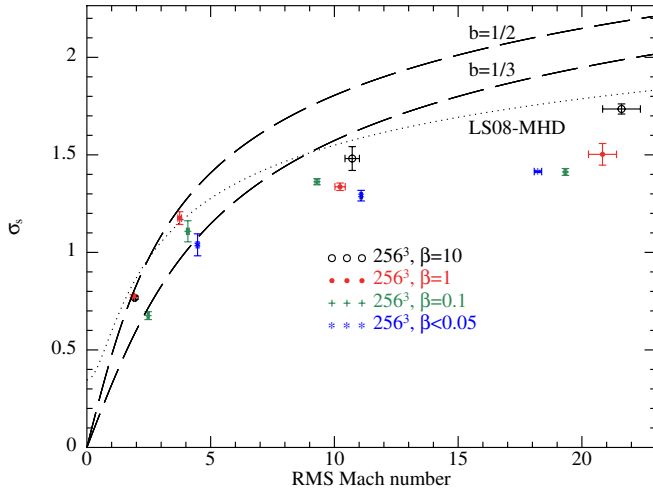


Figure 4. Same as Figure 1 but for a series of 256^3 grid-based MHD calculations with field strength characterized by the ratio of gas-to-magnetic pressure β (see the legend). There is a general decrease in the measured variance in the MHD simulations at high Mach number, though no clear trend with magnetic field strength. The best-fitting relationship found by LS08 for strong field MHD calculations (dotted line) is consistent with our $\beta = 1$ results in a similar parameter range ($\mathcal{M} \lesssim 6$), but too steep at higher \mathcal{M} . The $\beta < 0.05$ points refer to calculations employing $\beta = 0.05, 0.01$, and 0.02 at Mach 4, 10, and 20, respectively.

(A color version of this figure is available in the online journal.)

to explain the deviation from log-normality in the high density tail of the (column) density PDF. Magnetic fields do not help to explain the discrepancy.

We acknowledge computational resources from the Monash Sun Grid (with thanks to Philip Chan) and the Leibniz Rechenzentrum Garching. Plots utilized SPLASH (Price 2007) with the

new giza back end by James Wetter. C.F. is supported by Baden-Württemberg Stiftung grant P-LS-SPII/18.

REFERENCES

- Ballesteros-Paredes, J., Klessen, R. S., Mac Low, M.-M., & Vazquez-Semadeni, E. 2007, in *Protostars and Planets V*, ed. B. Reipurth, D. Jewitt, & K. Keil (Tucson, AZ: Univ. Arizona Press), 63
- Beetz, C., Schwarz, C., Dreher, J., & Grauer, R. 2008, *Phys. Lett. A*, **372**, 3037
- Brunt, C. M. 2010, *A&A*, **513**, A67
- Brunt, C. M., Federrath, C., & Price, D. J. 2010a, *MNRAS*, **403**, L507 (BFP)
- Brunt, C. M., Federrath, C., & Price, D. J. 2010b, *MNRAS*, **405**, L56
- Federrath, C., Klessen, R. S., & Schmidt, W. 2008, *ApJ*, **688**, L79
- Federrath, C., Klessen, R. S., & Schmidt, W. 2009, *ApJ*, **692**, 364
- Federrath, C., Roman-Duval, J., Klessen, R. S., Schmidt, W., & Mac Low, M. 2010, *A&A*, **512**, A81
- Hennebelle, P., & Chabrier, G. 2008, *ApJ*, **684**, 395
- Hennebelle, P., & Chabrier, G. 2009, *ApJ*, **702**, 1428
- Kainulainen, J., Beuther, H., Henning, T., & Plume, R. 2009, *A&A*, **508**, L35
- Klessen, R. S. 2000, *ApJ*, **535**, 869
- Kritsuk, A. G., Norman, M. L., Padoan, P., & Wagner, R. 2007, *ApJ*, **665**, 416
- Kritsuk, A. G., Norman, M. L., & Wagner, R. 2010, *ApJ*, **727**, L20
- Krumholz, M. R., & McKee, C. F. 2005, *ApJ*, **630**, 250
- Lemaster, M. N., & Stone, J. M. 2008, *ApJ*, **682**, L97 (LS08)
- Lombardi, M., Alves, J., & Lada, C. J. 2006, *A&A*, **454**, 781
- Lombardi, M., Lada, C. J., & Alves, J. 2008, *A&A*, **489**, 143
- Lombardi, M., Lada, C. J., & Alves, J. 2010, *A&A*, **512**, A67
- Nordlund, Å. K., & Padoan, P. 1999, in *Interstellar Turbulence*, ed. J. Franco & A. Carraminana (Cambridge: Cambridge Univ. Press), 218
- Padoan, P., Jones, B. J. T., & Nordlund, A. P. 1997a, *ApJ*, **474**, 730
- Padoan, P., & Nordlund, Å. 2002, *ApJ*, **576**, 870
- Padoan, P., & Nordlund, A. 2009, arXiv:0907.0248
- Padoan, P., Nordlund, A., & Jones, B. J. T. 1997b, *MNRAS*, **288**, 145
- Passot, T., & Vázquez-Semadeni, E. 1998, *Phys. Rev. E*, **58**, 4501
- Price, D. J. 2007, *PASA*, **24**, 159
- Price, D. J., & Federrath, C. 2010, *MNRAS*, **406**, 1659 (PF10)
- Scalo, J., Vázquez-Semadeni, E., Chappell, D., & Passot, T. 1998, *ApJ*, **504**, 835
- Schmidt, W., Federrath, C., Hupp, M., Kern, S., & Niemeyer, J. C. 2009, *A&A*, **494**, 127
- Vázquez-Semadeni, E. 1994, *ApJ*, **423**, 681